

Bohmian trajectories on a toroidal surface

Mario Encinosa ¹ and Fernando Sales-Mayor

Department of Physics

Florida A & M University

Tallahassee, Florida 32307

encinosa@cennas.nhmfl.gov, fsm@lanczos.cm.utexas.edu

Abstract

Bohmian trajectories on the toroidal surface T^2 are determined from eigenfunctions of the Schrodinger equation. An expression for the monodromy matrix $M(t)$ on a curved surface is developed and eigenvalues of $M(t)$ on T^2 calculated. Lyapunov exponents for trajectories on T^2 are found for some trajectories to be of order unity.

PACS No: 03.65.Ge, 05.45.Ac

Keywords: Bohmian, monodromy, chaos

The equation of motion for calculating Bohmian trajectories follows from inserting $\Psi(\mathbf{r}, t) = R(\mathbf{r}, t)e^{iS(\mathbf{r}, t)}$ into the Schrodinger equation and separating the ensuing expression into real and imaginary parts [1]. The result is ($m = \hbar = 1$)

$$\frac{d\mathbf{v}}{dt} = -\nabla(V + Q) \quad (1)$$

with $\mathbf{v} = \nabla S$ and Q the quantum potential

$$Q = -\frac{1}{2} \frac{\nabla^2 R}{R}. \quad (2)$$

Given a distribution of initial positions as determined from $\psi^*\psi$ the standard results of quantum mechanics are recovered.

This letter concerns the influence of curvature on Bohmian trajectories. Wu and Sprung [2] have pointed to the importance of a trajectory's initial position as critical to its evolution in time. If the trajectory lies on a curved surface, local curvature near the trajectory's initial position may be expected to play a role in its character. Here wave functions on a curved surface are employed to generate trajectories from S [2,3,4].

T^2 was chosen as the surface with which to investigate curvature effects on Bohmian trajectories for several reasons: First, the torus has non-trivial mean and Gaussian curvatures[5]. Second, good approximate wave functions for a particle on T^2 are available [6]. Finally, the rectangular strip $R^1 \times R^1$ with periodic boundary conditions can be used as a flat torus analog for comparison between trajectories on it and those on T^2 . For convenience the strip will be referred to as F^2 .

¹corresponding author

A toroidal surface with major radius R and minor radius a may be characterized by the Monge form

$$\mathbf{r}(\theta, \phi) = (R + a \cos\theta)\mathbf{e}_\rho + a \sin\theta \mathbf{e}_z \quad (3)$$

for which

$$ds^2 = a^2 d\theta^2 + (R + a \cos\theta)^2 d\phi^2. \quad (4)$$

The Hamiltonian is taken as $H = -\frac{1}{2}\nabla^2$. Defining $\alpha = \frac{a}{R}$, $\beta = 2Ea^2$, and making the standard $\chi(\phi) = e^{im\phi}$ ansatz for the azimuthal eigenfunction gives the Schrodinger equation

$$\frac{\partial^2 \psi}{\partial \theta^2} - \frac{\alpha \sin \theta}{[1 + \alpha \cos \theta]} \frac{\partial \psi}{\partial \theta} - \frac{m^2 \alpha^2}{[1 + \alpha \cos \theta]^2} \psi + \beta \psi = 0. \quad (5)$$

Eq. (5) was solved in [6] by a Fourier method. The explicit forms of the surface toroidal wave functions (STWs) used here are given in table I for $R = 1, a = 1/2$. The eigenfunctions on F^2 analogous to those in table I are $\begin{pmatrix} \cos n\theta \\ \sin n\theta \end{pmatrix} e^{im\phi}$.

As evidenced in table I, six STW states were chosen to comprise three positive parity states and three negative parity states. The $[nm]$ values selected for the negative parity states are the same as those selected for the positive parity states. This $[nm]$ matching was motivated by a desire to construct (as closely as possible) functions for comparison to $e^{in\theta}$ functions on F^2 . Additionally, without superpositions of the form $\psi_{nm}^+ \pm i\psi_{nm}^-$ some interesting motion about the minor radius of T^2 would not be manifest.

The phase S for T^2 and F^2 is generated with a six state superposition

$$\Psi(\theta, \phi, t) = \sum_{nm} c_{nm} \Psi_{nm}(\theta, \phi) e^{-iE_{nm}t}. \quad (6)$$

Trajectories were determined from

$$S = \tan^{-1} \left[\frac{Im\Psi}{Re\Psi} \right] \quad (7)$$

and

$$\frac{d\mathbf{r}}{dt} = \nabla S. \quad (8)$$

Eqs. (7) and (8) yield many classes of surface trajectories. Figures 1 and 2 give two state results for T^2 to the left of each figure and for F^2 to the right. Figure 3 shows a quantized trajectory structure that emerges from a combination of negative parity states on T^2 . Figure 4 is a $(\theta, \dot{\theta})$ plot for a path on T^2 showing rapid variation in phase space. Figure 5 is an example of a $(\theta, \dot{\theta})$ plot for a superposition with a dominant mode and small admixtures of two other states. A small change on the order of a few parts in 10^{-3} in θ_0 causes ample modification to the path. F^2 phase space plots have not been shown because they demonstrate (at least for the cases above) very little structure.

A measure of the divergence of two initially nearby trajectories is associated with the eigenvalues of the monodromy matrix $M(t)$ [7,8], used to good effect by Frisk [3] for the study of Bohmian paths on a two-dimensional rectangular geometry. $M(t)$ gives the time evolution of the separation vector $\delta\mathbf{x}$ via

$$\delta\mathbf{x}(t) = M(t)\delta\mathbf{x}(0). \quad (9)$$

Since

$$\frac{d}{dt}[\delta\mathbf{x}(t)] = \nabla[\delta S], \quad (10)$$

the monodromy matrix can be shown to obey the differential equation

$$\frac{dM}{dt} = JM. \quad (11)$$

For $R^1 \times R^1$ with or without periodic boundary conditions the J matrix is [3]

$$J = \begin{pmatrix} S_{xx} & S_{xy} \\ S_{yx} & S_{yy} \end{pmatrix}. \quad (12)$$

On a two dimensional surface characterized by a locally orthogonal metric

$$ds^2 = g_{uu}du^2 + g_{vv}dv^2$$

Eq. (12) must be extended to (written in a cumbersome but illustrative form)

$$J = \begin{pmatrix} \sqrt{g^{uu}} S_{uu} \sqrt{g^{uu}} & \sqrt{g^{uu}} S_{uv} \sqrt{g^{vv}} \\ \sqrt{g^{vv}} S_{vu} \sqrt{g^{uu}} & \sqrt{g^{vv}} S_{vv} \sqrt{g^{vv}} \end{pmatrix}. \quad (13)$$

On T^2 Eq. (13) yields

$$J = \begin{pmatrix} \frac{S_{\theta\theta}}{\alpha^2} & \frac{S_{\theta\phi}}{\alpha G} \\ \frac{S_{\phi\theta}}{\alpha G} & \frac{S_{\phi\phi}}{G^2} \end{pmatrix} \quad (14)$$

with $G \equiv 1 + \alpha \cos \theta$.

It is worth noting that for curved surfaces δ and ∇ do not commute. The ordering chosen in Eq. (10) insures all quantities lie on the local tangent space [9,10].

The differential equations implicit in Eq. (11) were found to be time consuming and slow to converge to suitable accuracy with standard methods on T^2 . Further, it was not clear that the results were accurate to any order. However, the foremost goal here was obtaining comparisons between the eigenvalues of $M(t)$ on T^2 versus those on F^2 for several values of θ_0 . With this in mind, a Mathematica code was set to solve the differential equations to a lower accuracy for the relatively short time $t = 10$. The advantages of adopting this procedure were a) confidence that our numbers were accurate to at least four significant digits and b) each point took only at most two minutes to acquire on an 800 MHz rated home PC [11].

Rather than work directly with the eigenvalues β_i of $M(t)$, a Lyapunov exponent λ_i is defined through the relation

$$\lambda_i(t) = \frac{1}{t} \ln \beta_i(t). \quad (15)$$

A more convenient definition which serves to dispense of an unknown overall norm is one employed in quantum Monte Carlo calculations [12] and adopted here,

$$\lambda_i = \frac{1}{(t_2 - t_1)} \ln \frac{\beta_i(t_2)}{\beta_i(t_1)}. \quad (16)$$

The larger of the two values of $\lambda_i \equiv \lambda$ was taken.

Tables II and III give values of λ as a function of θ_0 for two sets of c_{nm} values. For both sets λ is generally an order of magnitude larger on T^2 than on F^2 (save for one anomalous point). The F^2 values show a symmetry about $\theta = \pi$ while the T^2 values do not. The T^2 results certainly show dependence on θ_0 but do not show any simple relation to the Gaussian or mean curvatures K and H on T^2 . This is not unexpected. The Hamiltonian of Eq.(5) does not incorporate H and K explicitly but rather factors related to them in a complicated manner. A trajectory on T^2 generated from a representative point in table II is given in figure 6, and one from table III is shown in figure 7. Again, the corresponding F^2 plots do not possess enough structure to warrant their inclusion.

In this letter linear combinations of wave functions were employed to generate surface and phase space plots of Bohmian trajectories on T^2 and F^2 . The plots and tables illustrate that curvature can alter trajectory structure. This is a direct manifestation of the form of the wave functions on a curved surface. Each exponential function in a superposition of states on F^2 possesses its own time dependent energy phase while each STW is a superposition of several functions attached to one phase.

c_{nm} combinations making Lyapunov exponents on T^2 appreciably smaller than those on F^2 over many values of θ_0 have not been found. Positive λ of order unity is usually taken to indicate chaotic behavior, but while some trajectories are certainly complex, and λ an adequate measure of the distortion of local tangents, we consider it premature to state the trajectories are chaotic [13,14]. Nevertheless, it has been shown that a few low-lying states can yield complex phase space behavior on the the torus. Because the torus is a simple compact surface, its curvature likely causes less modification to trajectory structure than surfaces with rapidly varying regions of H and K . Those surfaces are certain to induce greater complexity in the trajectories.

Acknowledgments

The authors would like to thank Todd Timberlake for useful discussions. M.E. was partially supported by the NASA grant NAG2-1439 and F.S-M. by the Army High Performance Computing Research Center grant, cooperative agreement number DAAD 19-01-2-0014.

References

1. P. R. Holland, *The quantum theory of motion* (Cambridge University Press, Cambridge, 1993).
2. J. Wu and D.W.L. Sprung, Phys. Lett. A **261**, 150 (1999).
3. H. Frisk, Phys. Lett. A **227**, 139 (1997).
4. R.H. Parmenter and R.W. Valentine, Phys. Lett. A **201**, 1 (1995).
5. <http://mathworld.wolfram.com/Torus.html>
6. M. Encinosa and B. Etemadi, quant-ph 0200501 and submitted to Found. Phys. Lett.
7. F.H.M. Faisal and U. Schwengelbeck, Phys. Lett. A **207**, 31 (1995).
8. U. Schwengelbeck and F.H.M. Faisal, Phys. Lett. A **199**, 281 (1995).
9. R.W.R. Darling, *Differential forms and connections* (Cambridge University Press, Cambridge, 1994).
10. Reversing the order of ∇ and δ and projecting onto the tangent plane does not lead to a linear relation between $\delta x(t)$ and $\delta x(0)$.
11. The authors will supply the Mathematica source code upon request.
12. D. Ceperley and M.H. Kalos, *Monte Carlo methods in statistical physics*, K. Binder, Ed. (Springer Verlag Berlin, 1979).
13. D. Dürr, S. Goldstein and N. Zanghi, J. Stat. Phys. **68**, 259 (1992).
14. M.C. Gutzwiller, *Chaos in classical and quantum mechanics* (Springer-Verlag New York Inc. 1990).

Figure captions

Fig. 1. Trajectories for the superposition $\Psi(\theta, \phi, t) = \sqrt{\frac{2}{3}}\Psi_{32}^+ + i\sqrt{\frac{1}{3}}\Psi_{32}^-$ with $t = 30$ and $\theta_0 = 0$. The T^2 trajectory appears to the left of the figure. The F^2 trajectory projected onto the torus is to the right.

Fig. 2. Trajectories for $\Psi(\theta, \phi, t) = \sqrt{\frac{2}{3}}\Psi_{32}^- + i\sqrt{\frac{1}{3}}\Psi_{21}^+$ with $t = 24$ and $\theta_0 = 1.05\pi$.

Fig. 3. Trajectories for $\Psi(\theta, \phi, t) = \sqrt{\frac{5.2}{12}}\Psi_{21}^+ + (\sqrt{\frac{1.4}{12}}\Psi_{21}^- - i\sqrt{\frac{5.2}{12}})\Psi_{21}^-$ with $t = 50$ and $\theta_0 = 0$.

Fig. 4. $(\theta, \dot{\theta})$ plot for $\Psi(\theta, \phi, t) = \sqrt{\frac{1}{3}}\Psi_{21}^+ + i\sqrt{\frac{1}{3}}\Psi_{32}^+ - i\sqrt{\frac{1}{3}}\Psi_{32}^-$ with $t = 30$ and $\theta_0 = 1.25\pi$.

Fig. 5. $(\theta, \dot{\theta})$ plots for $\Psi(\theta, \phi, t) = \sqrt{\frac{0.02}{12}}\Psi_{10}^- + \sqrt{\frac{11.96}{12}}\Psi_{21}^- + \sqrt{\frac{0.02}{12}}\Psi_{32}^-$ with $t = 30$ and $\theta_0 = 1.424\pi$ shown on the left and for $\theta_0 = 1.429\pi$ shown on the right.

Fig. 6. $(\theta, \dot{\theta})$ plot for $\Psi(\theta, \phi, t) = \sqrt{\frac{1}{2}}\Psi_{32}^+ + \sqrt{\frac{1}{2}}\Psi_{32}^-$ with $t = 36$ and $\theta_0 = 0$.

Fig. 7. $(\theta, \dot{\theta})$ plot for $\Psi(\theta, \phi, t) = \sqrt{\frac{1}{2}}\Psi_{10}^+ + i\sqrt{\frac{1}{2}}\Psi_{10}^-$ with $t = 36$ and $\theta_0 = 0$.

Table I: Surface torodial wave functions and eigenvalues for $R = 1, a = 1/2$. Coefficients not listed are at least an order of magnitude smaller than those given.

$\Psi_{nm}^{\pm}; R = 1, a = 1/2$	β
$\Psi_{10}^+ = -.2176 + .4352 \cos\theta - .0714 \cos 2\theta + .0118 \cos 3\theta$	1.2223
$\Psi_{21}^+ = -.0733 + .2419 \cos\theta - .8393 \cos 2\theta + .0541 \cos 3\theta$	4.4767
$\Psi_{32}^+ = -.0420 + .1240 \cos\theta - .2772 \cos 2\theta + .8240 \cos 3\theta$	10.6657
$\Psi_{10}^- = +.8118 \sin\theta - .0739 \sin 2\theta$	0.9767
$\Psi_{21}^- = -.1799 \sin\theta - .8367 \sin 2\theta$	4.4106
$\Psi_{32}^- = -.0808 \sin\theta + .2568 \sin 2\theta - .8257 \sin 3\theta$	10.6151

Table II: Lyapunov exponents λ_9 measured at $t = 9$, λ_{10} measured at $t = 10$ and λ as defined by Eq. (16) for the superposition $\sqrt{\frac{1}{2}}\Psi_{32}^+ + \sqrt{\frac{1}{2}}\Psi_{32}^-$. The upper half of the table gives results for T^2 and the lower half are results for F^2 .

θ_0	0	$\frac{\pi}{6}$	$\frac{\pi}{3}$	$\frac{\pi}{2}$	$\frac{2\pi}{3}$	$\frac{5\pi}{6}$	π	$\frac{7\pi}{6}$	$\frac{4\pi}{3}$	$\frac{3\pi}{2}$	$\frac{5\pi}{3}$	$\frac{11\pi}{6}$
λ_9	2.12	4.23	2.53	1.91	3.36	2.29	2.75	2.55	3.11	1.72	1.23	2.70
λ_{10}	4.10	5.08	3.67	2.65	4.17	2.69	2.57	2.85	5.73	2.39	2.59	3.27
λ	21.9	12.7	13.9	9.35	11.5	6.35	.96	5.53	29.3	8.44	14.8	8.40
λ_9	.030	.036	.034	.033	.036	.032	.030	.036	.034	.033	.033	.036
λ_{10}	.047	.056	.050	.046	.049	.048	.047	.056	.050	.046	.046	.056
λ	.185	.234	.179	.161	.155	.195	.186	.233	.179	.160	.155	.235

Table III: Lyapunov exponents λ_9 measured at $t = 9$, λ_{10} measured at $t = 10$ and λ as defined by Eq. (16) for the superposition $\sqrt{\frac{1}{2}}\Psi_{10}^+ + \sqrt{\frac{1}{2}}\Psi_{10}^-$. The upper half of the table gives results for T^2 and the lower half are results for F^2 .

θ_0	0	$\frac{\pi}{6}$	$\frac{\pi}{3}$	$\frac{\pi}{2}$	$\frac{2\pi}{3}$	$\frac{5\pi}{6}$	π	$\frac{7\pi}{6}$	$\frac{4\pi}{3}$	$\frac{3\pi}{2}$	$\frac{5\pi}{3}$	$\frac{11\pi}{6}$
λ_9	2.46	1.69	1.68	1.63	1.67	1.86	2.01	3.59	3.64	3.22	3.13	6.87
λ_{10}	2.55	1.65	1.63	1.58	1.61	1.74	1.92	3.28	3.97	3.99	3.73	6.90
λ	3.39	1.23	1.02	1.19	1.07	.067	1.18	.447	7.00	10.90	9.14	7.16
λ_9	.086	.684	-.003	.022	.002	.009	.086	.684	-.003	.022	.002	.009
λ_{10}	.122	.336	.450	.124	.015	.032	.122	.336	.450	.124	.015	.032
λ	.415	-2.45	4.52	.942	.133	.239	.415	-2.45	4.52	.942	.133	.239

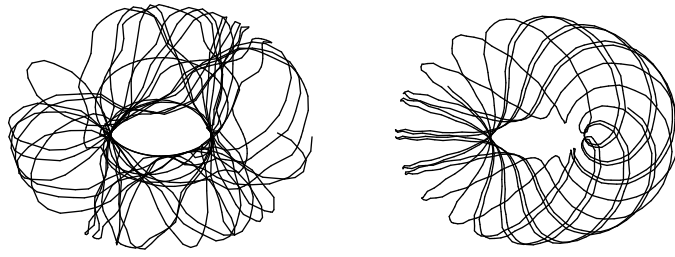


Figure 1:

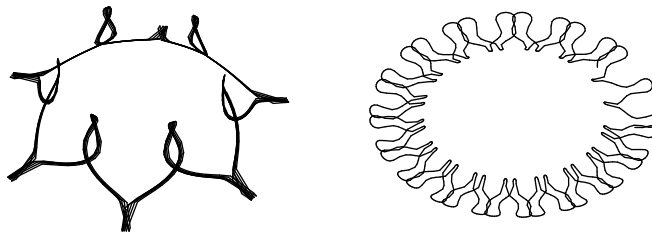


Figure 2:

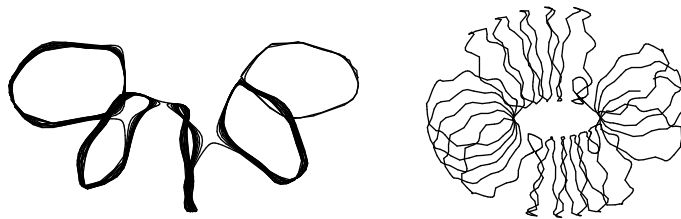


Figure 3:

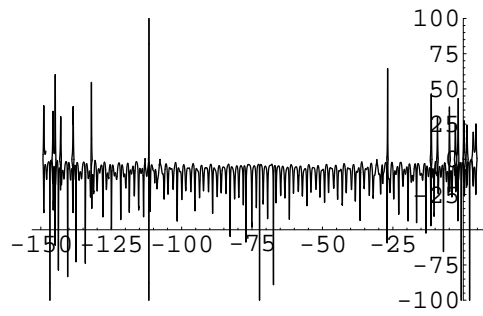


Figure 4:

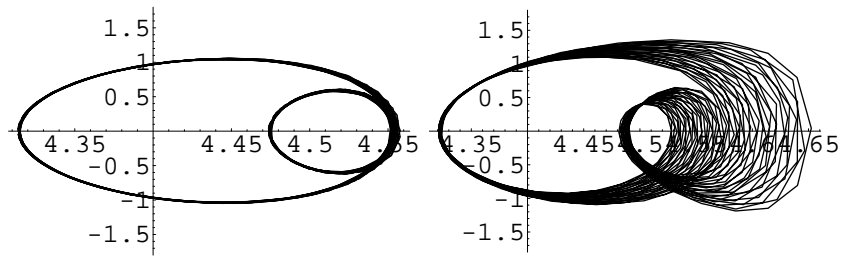


Figure 5:

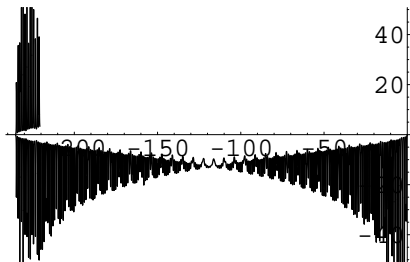


Figure 6:

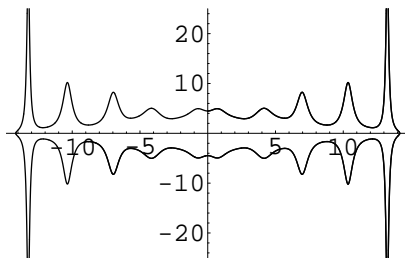


Figure 7: